The role of early bioelectric signals in the regeneration of planarian anterior/posterior polarity

Fallon Durant,[1] Johanna Bischof,[1] Chris Fields,[2] Junji Morokuma,[1] Joshua LaPalme,[1] Alison Hoi,[1], & Michael Levin[1*]

[1]Allen Discovery Center at Tufts University, and
Department of Biology,
Tufts University, Medford, Massachusetts

[2] 23 Rue des Lavandières,
11160 Caunes Minervois, France
ORCID: 0000-0002-4812-0744

[*] Author for Correspondence:
200 Boston Ave., Suite 4600
Medford, MA 02155
email: michael.levin@tufts.edu
ORCID: 0000-0001-7292-8084

Running title: Early bioelectric control of polarity

Keywords: planaria, regeneration, ion flux, bioelectricity, polarity, morphology, physiology

Abstract

Axial patterning during planarian regeneration relies on a transcriptional circuit that confers distinct positional information on the two ends of an amputated fragment. The earliest known elements of this system begin demarcating differences between anterior and posterior wounds by 6 hours post-amputation. However, it is still unknown what upstream events break the axial symmetry, allowing a mutual repressor system to establish invariant, distinct biochemical states at the anterior and posterior ends. Here, we show that bioelectric signaling at 3 hours is crucial for the formation of proper anterior/posterior polarity in planaria. Briefly manipulating the endogenous bioelectric state by depolarizing the injured tissue during the first 3 hours of regeneration alters gene expression by 6 hours post-amputation and leads to a double-headed phenotype upon regeneration despite confirmed washout of ionophores from tissue. These data reveal a primary functional role for resting membrane potential, taking place within the first 3 hours after injury, and kick-starting the downstream pattern of events that elaborate anatomy over the following 10 days. We propose a simple model of molecular-genetic mechanisms to explain how physiological events taking place immediately after injury regulate the spatial distribution of downstream gene expression and anatomy of regenerating planaria.

Introduction

Regeneration requires the reconstruction of complex anatomical structures and their appropriate integration with the remaining body via precise control of scaling, position, and organ identity. Planaria are free-living flatworms that have an incredible ability to regenerate missing tissue after damage and amputation despite having a rich set of internal organs, 3 body axes, and a complex brain and central nervous system (1-4), all of which must be recapitulated each time they regenerate. The process by which each wound blastema in a fragment decides what anatomical structure to form has been the subject of study for over 100 years (5, 6). Despite considerable progress on the genetics of stem cell differentiation and signaling pathways controlling these decisions (7-10), many gaps remain in our understanding of how tissue fragments are able to determine which cell types and body structures are missing and at which locations they need to be recreated (11, 12). This general question can be assessed most clearly in planaria by investigating the robust ability of cut fragments to establish proper anterior/posterior (AP) axial polarity (13, 14). This process includes three functional endpoints: forming the correct number of heads and tails, creating each one at the correct end with respect to the original orientation of the fragment within the host, and scaling new growth (and remaining soma) appropriately to regain proper overall proportions.

The current molecular models of AP polarity establishment in planaria involve feedback loops between Wnt signaling (15) and other genetic determinants of polarity, such as the ERK signaling pathway (16). Components of the Wnt pathway, *β-catenin* and *wnt-1*, both repress head formation and promote tail regeneration at posterior wounds in the regenerating planarian (17-22). Consequently, knockdown of *β-catenin* and *wnt1* both result in the growth of ectopic heads instead of tails. Furthermore, RNAi knockdown of known inhibitors of the Wnt pathway such as *axin* (23) and *APC-1* (18) induce two-tailed phenotypes.

Interestingly, most components of the Wnt pathway do not show differential expression along the AP axis early during regeneration. *Wnt1*, for

example, is expressed at both wounds of a middle fragment (20, 22, 24) and thus does not explain the differential fate of the two ends. Similarly, *hedgehog* signaling, which may in part regulate posterior-specific induction of *wnt* genes (25), seems to operate along the entire nervous system rather than only posteriorly (25). *Notum*, another inhibitor of the Wnt pathway (26), is the only known gene with an asymmetrical transcriptional response in the first 24 hours post-amputation (27). *Notum* expression first appears at the anterior blastema 6 hours after injury (27) and is required for the establishment of proper polarity (28). Notum has been shown to interact with β-catenin via negative feedback (28), but not much is known about what initially breaks the symmetry of the β-catenin/Wnt amplification loop leading to the early asymmetric expression of *notum (27)* and its subsequent repression of β-catenin (28).

In order to generate the large-scale AP patterning observed in fragments of planaria, the transcriptional circuits in individual cells need spatial inputs that provide positional cues with respect to the axes of the organism. What might be the input that breaks symmetry for the β-catenin/Wnt amplification loop with respect to the two wounds in a fragment, and ensures that the respective ends of the fragment acquire the correct anterior and posterior identities? In other systems, such as left-right axis establishment in vertebrates, upstream physiological signals drive transcriptional cascades that implement positional information; these pathways amplify small biophysical biases to align the differential expression of the earliest genes with the correct geometrical regions in the early embryo (29-31). Here we investigate the hypothesis that a similar system functions during AP axis specification during planarian regeneration.

One type of biophysical cue is the distribution of cell resting potentials across tissues *in vivo*, which feed into numerous downstream pathways during regenerative pattern control in a range of model systems (32-34). It is already known that bioelectric states are involved in planarian regenerative patterning (11), mirroring conserved roles for biophysical pathways in organ- and organism-scale patterning in vertebrate and invertebrate models (32-34). Classical gain-of-function experiments by Marsh and Beams (35-37) showed the reset of axial

polarity by applying external electric fields to regenerating flatworms (38, 39). More recently, imaging of endogenous bioelectric gradients (40-42) and loss-of-function strategies targeting ion channels, pumps, and gap junction proteins have implicated bioelectrics in planarian cell cycle regulation (43), control of head shape (44), size modulation (45), and stable as well as stochastic outcomes in AP polarity (40, 41, 46-48). However, it is not known how early the bioelectric signaling acts in this context.

To probe the events upstream of the first known asymmetric gene expression, we tested the hypothesis that the instructive membrane voltage (V_{mem}) differences that have been characterized at 24 hours post-amputation (40) are in fact established and operative far earlier. We used multiple ionophores to briefly and directly manipulate resting potential in regenerating fragments. Transient alterations of V_{mem}, which are only applied for the first 3 hours after regeneration, permanently impact subsequent gene expression and anatomical patterning events. We present a computational model of dynamic biophysical signaling that synthesizes the bioelectric and gene expression data to explain how bioelectricity works in concert with biochemical positional information systems to enable robust pattern homeostasis during regeneration. Overall, we show that difference in membrane voltage are detectable very early on during regeneration, before the first known differences in gene expression, and that transient, early disruption of membrane voltage can impact polarity establishment during regeneration. This indicates that physiological changes in membrane potential play an important role in the initial regulatory network which re-establishes polarity after injury in planaria.

Materials and Methods

Planarian colony care

A clonal strain of *Dugesia japonica (Dj)* was kept and maintained in accordance to Oviedo *et al.* (42) and were starved >7 days before all experiments were performed and continued to be starved for the duration of the experiment. Starvation is necessary to control the metabolic variability seen within individuals (42) and had no effect on regenerative speed or ability. Planaria at the beginning of each experiment were 5-15 mm in length before being amputated into fragments.

Ionophore treatment and amputations

Amputations were performed as in Nogi and Levin (48). Fragments posterior to the pharynx and half way between the tail tip (PT fragments) were made using a sharp scalpel and cut on a moistened cooled Kimwipe (Kimberly-Clark, New Milford, CT) and piece of black filter paper. Immediately after cutting, fragments were transferred to either a 0.24 µM nigericin (Adipogen) + 15 mM potassium gluconate (Sigma-Aldrich) solution (“nigericin solution”), or a 0.08 µM Monensin (Cayman Chemical Company) + 90 mM Sodium Gluconate (Sigma-Aldrich) solution (“monensin solution”). All reagents were titered for toxicity. 10 mM Nigericin and 7.2 mM monensin stock solutions were made by dissolving either nigericin or monensin in ethanol. Nigericin and monensin working solutions were then made by first dissolving potassium gluconate or sodium gluconate in commercial natural spring water (Poland Spring, Poland Spring Water, Framingham, MA), then adding nigericin or monensin stock to the appropriate concentration in the gluconate solutions. Control solutions contained corresponding amounts of ethanol in water (0.0024% and 0.0011% ethanol solutions respectively). Nigericin, monensin, and ethanol control solutions were removed 3 hours post-amputation, washed 3 times in water, and the animals were allowed to regenerate in groups of 30-40 worms at 20°C for the first seven days following amputation in deep-dish plates (100 x 20 mm; Fisherbrand; Thermo Fisher Scientific, Waltham, MA). Animals were then moved to 10°C to

prevent fissioning. Double-headed planaria were imaged 4 weeks post-amputation for morphometric analysis.

Evaluation of epidermal cell size

PT fragments were treated in a solution of 0.24 μM nigericin + 15 mM potassium gluconate or in a control solution with 0.0024% ethanol, combined with 300 nM Akita SS44DC dye (Akita Innovations, stock 1mg/ml in water) for 30 min. This dye efficiently labels cell membranes (49). Fragments were mounted in low-melt agarose and cells on the dorsal surface were imaged on a Nikon AZ100M Stereomicroscope. For each worm fragment, the area of 20 cells that had clear boundaries were measured using the “Measure” function in Fiji software. Number of pixels used in the “Measure” function was converted to μm in Fiji. Quantitative data resulting from this analysis is presented in Supplemental Data.

Phenotype scoring and statistical analysis

Scoring was performed using a Zeiss SV6 dissecting microscope (Oberkochen, Germany). Criteria for a double-headed phenotype were at least one eye on each of the anterior and posterior poles. Samples were allowed to regenerate until at least day 14 before scoring. Sample sizes reflected in text are pooled from at least three replicate experiments over the course of several months.

In situ hybridization

Animals were fixed in formaldehyde-based solution for whole-mount *in situ* hybridization as in Pearson *et al. (50)* using the probe Dj *notum*. The partial codon of Dj *notum (accession number* MH000608) was synthesized (GeneArt, Thermo Fisher Scientific, Waltham, MA), based on the sequence homology from the RNA-seq data used in Chan *et al.* (51) and was cloned into a vector pCRII-TOPO (Thermo Fisher Scientific, Waltham, MA). Against this, the *in situ* probe

was generated against the full-length clone, and was hydrolyzed to a shorter length for better penetration.

Gene knockdown with RNA interference

Double-stranded RNA (dsRNA) was synthesized as in Rouhana *et al.* (52) and injected as in Oveido *et al. (53)*. DJ *β-catenin* dsRNA (47) was injected on days 1-3 and worms were cut on day 7 into 5 pieces as shown in (47). For V_{mem} imaging, animals were imaged in $DiBAC_4(3)$, as below, 3 hours post-amputation. Double-headed worms were imaged for morphometric analysis 4 weeks post-amputation.

Membrane voltage reporter assay

Bis-[1,3-dibarbituric acid]-trimethine oxanol ($DiBAC_4(3)$; Invitrogen, Carlsbad, CA) was used for all membrane voltage reporting assays as in Adams *et al. (54)* and Oviedo *et al.* (42). Planaria were amputated as above to produce PT fragments that were treated in nigericin, monensin, or control ethanol solutions. 3-hour time point animals were treated in drug with added $DiBAC_4(3)$ immediately after amputation and remained in the same solution for membrane voltage imaging at 3 hours post-amputation. 6-hour time points were removed as above, washed into water, and placed in a $DiBAC_4(3)$ solution a half hour before imaging. Wild type, untreated animals used in experiments to describe the timeline of bioelectric signaling within the first 24 hours of regeneration were also soaked in a $DiBAC_4(3)$ solution for a half hour before imaging. Planaria were immobilized using 2% low melting point agarose and Planarian Immobilization Chips (55). Ethanol-treated controls were imaged side by side on the same chip in tandem with ionophore-treated animals, ventral side up so that direct comparisons between pairs could be made. Animals were tracked individually in multiwell, non-treated cell culture plates (24-well; Greiner Bio-One, Monroe, NC). Functionality of $DiBAC_4(3)$ was verified recently in (40). Voltage profiling data are limited to the outermost layer of cells due to opacity of pigmentation of planarian tissues.

Image collection and processing

Membrane voltage images were collected using a Nikon AZ100M Stereomicroscope (Melville, NY) with an Andor Technology DL-604M VP camera (South Windsor, CT), using an epifluorescence optics FITC filter (GFP HC: 470/40, 495, 525/50). Images were pseudocolored using NIS-Elements imaging software (Nikon). Original black and white images were flat-field corrected using the software Fiji (56). All other images were collected using a Nikon SMZ1500 microscope with a Retiga 2000R camera (Qimaging, Surrey, BC, Canada) and Q-Capture imaging software (Qimaging). Adobe Photoshop (Adobe Systems, San Jose, CA) was used to organize figures, rotate and scale images, and improve visibility of entire image with the exception of the membrane voltage images, which were unaltered for brightness.

Statistics and analysis of membrane voltage reporter assay data

Quantitative comparisons of anterior versus posterior blastemas and ionophore-treated versus control ethanol-treated animals were performed using Fiji (56). To evaluate differences between blastemas, a selection box measuring 15x30 pixels was aligned at the anterior and posterior blastemas and average intensity was quantified using the “Measure” function. For the ionophore and *β-catenin* dsRNAi $DiBAC_4(3)$ experiments, the area of each entire fragment was selected, and average intensity was quantified using the “Measure” function. Both analyses were performed in the software after background and flat-field image corrections. Statistical comparisons between anterior and posterior blastemas and between ionophore- and ethanol-treated animals (as well as a control versus control comparison) were made using Microsoft Excel to calculate Student’s *t*-test (two-tailed distribution, paired samples, unequal variance). Before running each t-test, each dataset was verified to be normally distributed using the Shapiro-Wilk test using a p=0.01 threshold. All quantitative data can be found in Supplementary Data.

Morphometric analysis

Worms were relaxed with ice water and imaged using a Nikon SMZ1500 microscope (Melville, NY, USA) with a Retiga 2000R camera (Surrey, BC, Canada) and Q-Capture imaging software (Surrey, BC, Canada). Landmark data were then recorded using ImageJ (Bethesda, MD, USA) (57). Landmarks were chosen as in Emmons-Bell et al. (44) and included an extra landmark on each side to indicate ridges formed by improper scaling phenotypes or smooth transition from head to body. MorphoJ (Manchester, UK) (58) was used for Principal Components Analysis, in order to quantify and graphically represent changes in scaling morphology. MorphoJ was also used to calculate Procrustes distances and perform statistical analyses.

Predictive modeling

An interactive simulation tool implementing the model of wound blastema response to bioelectric state described below was developed using javascript and HTML Canvas. The wound-response model calculates quantitative head and tail regeneration probabilities for anterior and/or posterior amputations transverse to the AP axis as functions of the bioelectric state of the wound blastema. The simulation tool runs this model for simulated amputation experiments for which the initial bioelectric state of the intact animal, amputation position(s) along the AP axis, bioelectric response to amputation, and external (e.g. drug-induced) modifications of V_{mem} at wound blastema can be manipulated as parameters. This simulation tool can be manipulated and its source code examined at https://chrisfieldsresearch.com/bcar-model.htm.

Chemical analysis of ionophore washout

Worms were flash frozen without any liquid and stored at -80°C until preparation. For preparation for LC/MS analysis, samples were thawed; 3 mm glass beads (Milipore) were added to the tissue before vortexing for 1 minute. Ethanol was added as a solvent and samples were vortexed again. Liquid phase was removed and centrifuged for 20 minutes at 14,000 rpm at 4°C. The upper

clear phase was removed and filtered through a 0.2 µm PTFE-S filter (Whatman). Samples were stored at -80°C before analysis. The standard solution was 1 mM nigericin or monensin in 100% ethanol.

Detection of nigericin and monensin by LC/MS (Harvard FAS Core Facility, Cambridge, MA) was carried out on a Thermo Scientific Dionex UltiMate 3000 UHPLC coupled to a Thermo Q Exactive Plus mass spectrometer system (Thermo Fisher Scientific Inc, Waltham, MA) equipped with an HESI-II electrospray ionization (ESI) source. Data were acquired with Chromeleon Xpress software for UHPLC and Thermo Xcalibur software version 3.0.63 for mass spectrometry, and processed with Thermo Xcalibur Qual Browser software version 4.0.27.19.

A 5 µL sample was injected onto the UHPLC including a HPG-3400RS binary pump with a built-in vacuum degasser and a thermostatted WPS-3000TRS high performance autosampler. A Symmetry Shield RP18 analytical column (2.1x150 mm, 3.5 µm) from Waters Corporation (Milford, MA) was used at the flow rate of 0.3 mL/min using 0.2% acetic acid in water as mobile phase A and 0.2% acetic acid in methanol as mobile phase B. The column temperature was maintained at room temperature. The following gradient was applied: 0-2.4 min: 0% B isocratic, 2.4-3.4 min: 0-70% B, 3.4-4.4 min: 70-100% B,4.4-8.4 min: 100% B isocratic, 8.4-8.5 min: 100-0%B, 8.5-13.5 min: 0% B isocratic.

The MS conditions were as follows: negative ionization mode for all targets; full scan mass range, m/z 60 to 850; resolution, 70,00; AGC target, 1e6; maximum IT, 220 ms; spray voltage, 3500 V; capillary temperature, 280 ˚C; sheath gas, 47.5; Aux gas, 11.25; probe heater temperature, 412.5 ˚C; S-Lens RF level, 50.00. A mass window of ± 5 ppm was used to extract the ion of $[M-H]^-$ for all the targets. Targets were considered detected when the mass accuracy was less than 5 ppm and there was a match of isotopic pattern between the observed and the theoretical samples and a match of retention time between those in real samples and standards.

Results

Bioelectric differences between anterior and posterior blastemas are detectable before asymmetric anterior gene expression

Previous work has shown that bioelectric signaling changes along the anterior/posterior (AP) axis of regenerating planaria as early as 24 hours after amputation (41), it was not known how early this difference is established. We used $DiBAC_4(3)$, a voltage reporting dye, to assay voltage differences between the anterior and posterior blastema as early as one hour post-amputation. Although currently the technology does not permit us to quantitatively determine absolute V_{mem} for planarian cells, we were able to determine relative comparisons of V_{mem} between samples or within the same worm fragment.

Even at the earliest time points assayed (1h after amputation), regardless of cut location along the AP axis, anterior blastemas were more depolarized than the posterior blastemas of adjacent fragments (Figure 1A). Similarly, the significant differences between anterior and posterior blastemas on the same fragment seen at 3 hours after amputation (Figure 1Ba, quantified in C) persisted at 6, 12, 18, 24, and 48 hours after amputation (Figure 1Bb-d, quantified in C).

The earliest previously-described distinguishing factor between anterior and posterior blastemas in planaria, as determined by RNASeq profiling, is asymmetric expression of the gene *notum* which first becomes detectable at 6 hours post-amputation (27). This early asymmetry is crucial for establishing proper head-tail formation in regenerating *Schmidtea mediterranea*, a closely related planarian species (28). Thus, we hypothesize that *notum* expression follows a similar timeline during head-tail axis establishment in *Dugesia japonica*. In order to characterize the transcriptional response of *notum* during early regeneration in *Dugesia japonica*, we first identified the *Dugesia japonica* homologue of *notum* and characterized its expression pattern relative to the time course of bioelectric state changes after amputation described above. *In situ* hybridization for *Dj-notum* RNA showed a similar expression pattern to that found in *Schmidtea mediterranea* (59, 60). No expression at either blastema was

detectable before or at 3 hours post-amputation, the timepoint at which we observed a significant depolarization of the anterior blastema relative to the posterior blastema (Figure 1Da & b). Higher levels of *notum* expression at the anterior blastema as compared to the posterior blastema were observed at 6 hours post-amputation (Figure 1Dc). *Notum* expression at 12, 18, and 24 hours post-amputation also corresponded to what has been previously found in the literature in *Schmidtea mediterranea* (28) (Supplemental Figure 1A). Although there may be earlier differences in expression of other genes that have yet to be discovered (ones that can function at expression levels below detection even by RNASeq) and there are possibly other earlier cellular events that may play a role in early axial establishment (including phosphorylation), we conclude that bioelectric asymmetries between the anterior and posterior blastemas occur prior to the earliest asymmetric gene known to be expressed, *notum*.

Early alteration of bioelectric state results in robust changes to anterior/posterior polarity

To determine whether the early bioelectric state of planarian tissue is functionally important for proper establishment of anterior/posterior polarity after regeneration, we sought to directly alter the resting potential of cells. We chose to alter the resting potential via ionophore treatment rather than RNAi against channel and pump proteins, in order to avoid disruption of any potential non-bioelectric roles of channels or pump proteins. We exposed fragments to the potassium ionophore nigericin (61) in combination with potassium gluconate to optimize depolarization of the tissue. Fragments cut posterior to the pharynx and anterior to the tail (PT fragments) were soaked in 0.24 µM nigericin + 15mM potassium gluconate solution immediately after cutting for 3 hours before switching them to water (Figure 2A). As expected, at 3 hours post-amputation, nigericin solution-treated fragments were significantly depolarized compared with fragments treated in control solution (0.0024% ethanol in water) (Figure 2Bd, as compared to 2Ba and quantified in 2Bg, alternate quantification in Supplemental Figure 2A and 2B). Any potential osmotic effects of incubation in the nigericin

solution was tested by measuring the size of cells in the epidermis in nigericin solution-treated fragments versus control solution treated fragments. Consistent with published data showing significant edema and regenerative failures induced by osmotic shock, we observed no difference in the size of the cells (Supplemental Figure 3A, quantified in 3B), indicating that the difference in osmolarity between the solutions is unlikely to explain the observed phenotype.

The observed depolarization induced by short-term incubation in nigericin solution (Fig 2Bd, compared to 2Ba) resulted in the regeneration of double-headed planaria in 13% of observed worms (Fig 2Bf) compared to 0% in controls (Figure 2Bc). The remaining 87% of animals regenerating in nigericin solution formed morphologically normal single-headed worms, indistinguishable from controls, with no intermediate phenotypes.

Double-headed planaria were also produced by pre-soaking animals in potassium gluconate without added nigericin for a week before amputation (8%, N=60, of regenerated treated worms compared to 0% of regenerated worms in controls), revealing that the induced patterning changes were not due to any secondary effects of nigericin. We hypothesize that pre-soaking of the animals is required in the absence of ionophore to allow time for high potassium levels in the external medium to propagate past the protective integument and into the interstitial milieu of the animal so as to affect the V_{mem} of deep tissues. Thus, we conclude that patterning of double-headed planaria can result from a transient bioelectric signal that is converted into stable biochemical and anatomical consequences.

We next asked whether the induction of the double-headed state was a specific consequence of nigericin or of changes in V_{mem} in general. To test the ionophore dependency of these treatment outcomes, we treated fragments with the sodium ionophore monensin (62) and sodium gluconate to increase the intracellular sodium levels and thereby depolarize the cells (Figure 2A). Exposure of fragments to 0.08 μM monensin + 90 mM sodium gluconate for the first 3 hours of regeneration resulted in significant depolarization compared to fragments treated in the control solution (0.0011% ethanol in water) (Figure 2Ca

versus 2Cd and quantified in 2Cg, alternate quantification in Supplemental Figure 2A and 2C). As observed for regeneration in nigericin solution, exposure of fragments to monensin solution also led to regeneration of double-headed worms (12% of treated worms compared to 0% of controls) (Figure 2Cf as compared to 2Cc). Because manipulating either the potassium concentration gradient or sodium influx resulted in double-headed worm phenotypes, we conclude that this phenomenon is dependent on depolarization of the tissue regardless of the mechanism that triggers it..

A Model Integrating Planarian Bioelectrics and Regenerative Outcomes

To understand and control regeneration, it is important to derive the rules underlying patterning outcomes as a function of physiological state. To achieve this, we constructed a quantitative, computational model of AP axis determination in planaria regeneration based on data from the literature and current findings (Figure 3). An interactive, quantitative simulation tool of the described model is available at https://chrisfieldsresearch.com/bcar-model.htm. Example quantitative predictions using this tool have been included in Supplemental Tables 1 and 2.

The model assumes that in a normal, regenerating wild-type worm, there is a distribution of V_{mem} across the AP axis such that the worm is more depolarized at the anterior and more hyperpolarized at the posterior (41). Upon amputation, cells that will form the somatic component of the wound blastema are exposed to a local Ca^{++} spike from cell debris. The model assumes that these cells respond to higher local Ca^{++} by opening Ca^{++} channels in a V_{mem}-dependent way, with depolarized cells opening more Ca^{++} channels and hence undergoing further depolarization while hyperpolarized cells open fewer Ca^{++} channels and remain hyperpolarized; this assumption is consistent with observations of Ca^{++} response in both planaria (41, 63, 64) and other systems (65-67). The net result of this V_{mem}-dependent response to Ca^{++} release due to wounding is that the AP V_{mem} distribution in the amputated fragment is amplified to approximately replicate the AP V_{mem} distribution of the intact animal. The blastema cells then compare their current V_{mem} state with the nearby non-blastema cells via gap junction

communication. These nearby cells are assumed to be in the interior of the fragment rather than on the surface. Voltage gating and electrophoretic effects mediated by gap junction communication between adjacent cells allow small molecule signaling to occur differentially depending on the relative voltage states of the two connected cells (reviewed in (68-70)).

Whether the Brain/Head pathway or the Tail pathway becomes implemented by a wound blastema is quantitatively determined by the depolarization difference between blastema cells (V_B) and their near neighbors in the interior of the fragment (V_{int}), with a large depolarization difference activating the Brain/Head pathway and a small or negative difference activating the Tail pathway (Fig. 3A). Letting $\Delta V = V_B - V_{int}$, the Brain/Head activation probability is modeled by a sigmoid response function:

$$Prob(\text{Brain/Head}) = \text{Brain/Head Activation} = 1 / (1 + e^{-\alpha(\Delta V - V_{exp})})$$

where the adjustable parameter α (default = 0.8) represents the precision of Vmem comparisons and the adjustable parameter V_{exp} represents the baseline or "expected" ΔV. The Tail activation probability is 1 – *Prob*(Brain/Head). The pathway decisions at the two wound blastema depend only on the local depolarization difference ΔV and are completely independent of each other.

Consistent with the observations reported here, activation of the Brain/Head pathway is assumed to linearly induce *notum* expression at low to intermediate depolarization with sigmoidal saturation at high depolarization; similarly, activation of the Tail pathway is assumed to linearly induce *β-catenin* expression (Figure 3A). Local mutual inhibition by Notum and β-catenin is assumed, in the model, to assure a winner-take-all decision by each blastema to activate either the Brain/Head or the Tail pathway, preventing regenerates in which both Head and Tail components are regenerated at a single wound blastema; however, this cell-population level dynamic is not modeled explicitly.

In an ionophore-treated animal, exposed cells at both wounds become similarly depolarized and similarly increase their depolarization in response to increased Ca^{++} at the wound site, in which case both wound blastemas are more

depolarized when they compare their current state with the non-blastema cells (Figure 3B). This leads to the initiation of the Brain/Head pathway, although whether the Brain/Head pathway is fully executed to produce a phenotypically normal brain and head may depend on multiple downstream events.

On a molecular level, a local, concentration ratio-dependent Notum/β-catenin mutual inhibition is consistent with the previously published Tail pathway activation by dsRNAi-mediated knockdown of *notum* at both anterior and posterior wounds and Brain/Head pathway activation at both wounds enabled by *β-catenin* knockdown (28). Expression of both *notum* and *β-catenin* is predicted to be quantitatively inactivated by excessive blastema depolarization (Fig. 3B). As all cells would be expected to activate the Brain/Head pathway in a highly-depolarized wound blastema, inhibition of the Tail pathway by *notum* would not be necessary to prevent tail regeneration in this case. Therefore, we next tested our model's prediction that depolarization induced by nigericin treatment should reduce overall *notum* expression.

Early alteration of V_{mem} changes *notum* expression pattern

Previous work has shown that expression of *notum* is completely absent from the double-headed worms produced by *β-catenin* knockdown (28). Our model suggests that this absence is due to the primary function of *notum* as a means of inhibiting Wnt signaling at anterior wounds rather than a function as a patterning initiator, and due to the presence of a feedback loop (28), the absence of Wnt signaling results in a lack of *notum*. We predicted that in fragments treated with nigericin solution, both blastemas would be heavily depolarized, wiping the physiological asymmetry seen in early regenerating fragments. Our model predicts that in this scenario the Brain/Head pathway would activate on each end of the worm and *notum* expression would not occur. We tested this hypothesis by exploring how a 3-hour nigericin solution treatment would affect *notum* expression in regenerating fragments.

As shown above, in a normal regenerating planarian, at 3 hours post-amputation, the anterior blastema is depolarized relative to the posterior

blastema (Figure 4Aa), while *notum* is not expressed anywhere in the fragment (Figure 4Ca, 100%, N=20). At 6 hours post-amputation, the depolarized anterior blastema remains (Figure 4Ab) and *notum* is expressed asymmetrically at the anterior end of the fragment (Figure 4Cb, 89%, N=37). This leads to the regeneration of a worm with normal anterior/posterior polarity. When a regenerating planarian is exposed to a depolarizing solution of nigericin for the first 3 hours of regeneration, at 3 hours post-amputation the anterior blastema is depolarized relative to the posterior blastema (Figure 4Ac, quantified in B) as is observed in controls. However, at 6 hours post-amputation, unlike controls, the depolarization between the anterior and posterior blastema is indistinguishable (Figure 4Ad, quantified in B). This occurs even though nigericin is washed out after the first 3 hours after amputation and is no longer detectable in the tissue at 6 hours (Supplemental Figure 4). At the 3-hour timepoint *notum* is not expressed in controls and is not expressed until the 6 hour timepoint (Figure 4Ca & b, 100%, N=30). Nigericin solution treated animals similarly do not express notum at the 3-hour timepoint (Figure 4Cc, 100%, N=30), but strikingly, correlative with blastema depolarization, *notum* fails to begin its normal expression at 6 hours post-amputation in a majority of animals (Figure 4Cd, 85%, N=27). Given that this same treatment creates ectopic heads, this is consistent with previously published work describing an absence of *notum* expression in the ectopic heads induced by β-catenin RNAi (28). These data collectively suggest that early depolarization disrupts the polarization of the two blastemas, destabilizes the events that lead to AP axis establishment, and leads to an increased rate of regeneration of double-headed worms. We conclude that bioelectric state facilitates expression of *notum* and may influence other downstream targets participating in regenerative control.

AP polarity and scaling are independently regulated by V_{mem} and *β-catenin*

Our model predicts, consistent with the *notum* expression data, that V_{mem} plays an important role in the early regulation of *wnt*-dependent signaling that establishes AP polarity in planaria. To examine possible relationships between

these signals, we checked V_{mem} signatures in double-headed animals induced via *β-catenin* RNAi knockdown (Figure 5A). A key comparison between *β-catenin* dsRNAi-induced double-headed worms and those induced by nigericin treatment concerns the scaling of the new tissue relative to the fragment, which is a crucial aspect of regenerative response (6, 71-73). Despite the same timeframe of regeneration, the double-headed worms induced by β-catenin inhibition were improperly scaled, with newly regenerated heads being well-formed and complete, but conspicuously smaller than the original heads and remaining body (Figure 5Ba). These observations were not seen in nigericin treated animals (Figure 5Bb) and could not be rescued by co-treating *β-catenin* dsRNAi-injected animals with nigericin solution (Figure 5Bc). This indicates that while V_{mem} regulates AP polarity, *β-catenin* is likely to serve not only AP polarity but also tissue scaling during regeneration, as both are disrupted upon its inhibition.

Importantly, we also observed that fragments from worms injected with *β-catenin* dsRNAi did not show a difference in V_{mem} compared to control worms (Figure 5Ca & b) in contrast to the depolarization observed in fragments treated with nigericin solution (Figure 5Cc, quantified in D), even though both *β-catenin* dsRNAi and nigericin treatment lead to formation of double-headed worms (Figure 5B). The fact that *β-catenin* knockdown does not significantly affect bioelectric profiles suggests that β-catenin signaling is not upstream of V_{mem} in this context.

The observation that double-headed worms resulting from nigericin solution-induced depolarization exhibited heads that were correctly proportioned to the rest of the body was confirmed using quantitative morphometrics. Head morphology differences between *β-catenin* RNAi animals and nigericin-treated animals were deemed significant (Figure 5E) whereas combining *β-catenin* dsRNAi with nigericin solution treatment gave rise to double headed worms that were quantitatively indistinguishable from those induced by *β-catenin* dsRNAi on its own (Figure 5E, Procrustes ANOVA, $p>0.05$) using the landmarks as defined (Figure 5F). Thus, depolarization cannot rescue the improper scaling induced by

β-catenin dsRNAi, suggesting that while V_{mem} depolarization gives rise to correctly-scaled heads, it cannot do so if *β-catenin* signaling is disrupted.

Discussion

Bioelectric physiology is an important component of repair and regeneration in numerous model systems (33, 54, 74-81). Endogenous bioelectric fields have been shown to regulate many patterning, morphological, and regenerative processes (33, 82-86) and to serve as instructional pre-patterns (87, 88). In planaria, changes in bioelectric physiology can alter the AP polarity of the worm (41), create changes in head size and shape (44, 45), create stable but stochastic heteromorphoses that appear on subsequent rounds of amputation (40). Here, we show that in normal regenerating planaria the anterior blastema is depolarized relative to the posterior blastema, and that this early depolarization occurs quickly, arising within the first hour after amputation and persisting through 48 hours after amputation. This is consistent with an early role for bioelectric signaling in regulating the reformation of polarity, as the first known polarized gene expression, that of *notum,* is detectable only after 6 hours post-amputation. Although there may be earlier cellular events that contribute to axial establishment, such as phosphorylation, or asymmetrical transcription of genes that are undetectable by the most sensitive methods currently available, our work indicates that physiological bioelectric signals are observable earlier in the regenerative timeline than any known downstream regulatory networks.

β-catenin has been firmly established as an important regulatory element in the definition of head versus tail identity (17-19, 89) and inhibition of *β-catenin* has been long known to create double-headed worms in planaria (18). Our model predicts that V_{mem} lies upstream of regulating AP polarity through *β-catenin,* as confirmed by our observations that *β-catenin* knockdown does not induce differences in V_{mem} patterns compared to controls. Thus, we propose that depolarization induces changes to *β-catenin* signaling which leads to downstream changes in anatomical patterns. The functional data make clear that these physiological signals are important and instructive from the earliest

moments of regeneration. Future work testing known transduction mechanisms by which bioelectric state change regulates downstream transcription (90) will address the question of precisely how V_{mem} activates the subsequent genetic targets.

The inability for depolarization to rescue the scaling phenotypes observed with concomitant β-catenin RNAi suggests that proper scaling, as observed in depolarization-induced ectopic heads, requires the function of β-catenin. This is not to say that signaling downstream of V_{mem}-dependent changes cannot impact scaling at later timepoints in a β-catenin dependent manner, as supported by previous work on the bioelectric determinants of size control (45, 91). *β-catenin* signaling has many inputs and outputs, and it is also possible that compensatory mechanisms later in the regenerative timeline could be reinstating proper scaling in some scenarios. It is an exciting prospect to further explore these potential new roles for *β-catenin*-dependent scaling and its relationship to V_{mem} alterations in the future.

We developed a model to explain the observed coordination of bioelectric signals with the molecular feedback loops that are important in early anterior/posterior axis establishment. Our model made the fundamental prediction that expression of *notum* would be inactivated by excessive blastema depolarization such as that seen with nigericin solution treatments. The lack of *notum* expression in our model is due to all cells' activating the Brain/Head pathway in highly-depolarized wound blastemas, predicting that *notum* expression would not be necessary to prevent tail regeneration at anterior blastemas and leading to double-headed planaria. This is consistent with the observed double-headed phenotype and absence of *notum* expression upon knockdown of *β-catenin* (Petersen and Reddien, 2011); when the Tail pathway/β-catenin signaling is inhibited, *notum* does not need to be expressed so as to limit *β-catenin* expression in the anterior part of the worm. We confirmed this prediction by showing that *notum* was not expressed in early, nigericin solution-depolarized regenerates. One implication is that the role of asymmetric *notum* expression at the anterior blastema may not be to activate the Brain/Head-

pathway, but rather that endogenous levels of depolarization at the anterior blastema are responsible for activating the Brain/Head-pathway and *notum* serves as a way to maintain the execution of this pathway by inhibiting posterior signaling very early on in regeneration.

Our experiments revealed an interesting temporal aspect of bioelectric change. Consistent with observations in the literature suggesting that both depolarizing agents used in this work, nigericin and monensin, are washable from treated tissue (92-95), we observed that while nigericin and monensin rapidly leave the worms' tissues upon washout, the induced changes in V_{mem} and AP polarity persist. This suggests the existence of a feedback signaling system that allows the maintenance of the depolarized state after the initial trigger is removed. Previous experiments have shown that these maintained, altered bioelectric states have the ability to store altered body plans that stochastically appear upon subsequent rounds of amputation (40). The system maintaining the bioelectric state likely relies on a combination of changes to downstream gene expression or protein modifications (96-98), alterations in gap junctional connectivity and ion channel states (12, 79, 99-104). This shows parallels to mechanisms known to drive either intrinsic or synaptic plasticity in the brain, where global modulation of neural networks occurs by modification of voltage gated ion channels (reviewed in (105)).

Overall, our data reveal that bioelectric signals play an early role in determining polarity in regenerating fragments through the downstream regulatory networks leading to patterned expression of position control genes (25, 27). This offers avenues for manipulating large-scale anatomical outcomes in regenerative settings via manipulating membrane potential (81, 106), as illustrated here by the induction of double-headed regenerative outcomes through the depolarization of the entire fragment, and recently shown in vertebrate models (81).

It is important to note that current tools for detecting changes in V_{mem} can only visualize surface changes in planaria due to strong pigmentation of the epidermis. We anticipate that important events are occurring in deeper tissues.

When comprehensive physiomic profiling data become available, it may become possible to extract from the V_{mem} data much more detailed patterning information than merely head-tail instructions. Future work and advances in bioelectric effector methodology and techniques borrowed from the neural decoding field (107, 108) will enable probing more deeply into the mechanisms behind cell networks' long-term and dynamic responses to induced changes in V_{mem}.

Conclusion

Physiological circuits integrate with canonical signaling networks; understanding this interplay is key for a full understanding of the time dependence and complexity of regeneration and for harnessing control over regenerating systems. In planaria, upon injury, the bioelectric state shifts in a polarized manner establishing an anterior-posterior axis at an extremely early timepoint. These bioelectric events play an important determinative role in polarity decisions. Future development of optogenetic tools allowing for fine-scale control over V_{mem} patterns will enable this model system to play an important role in decoding the relationship between complex physiological patterns and molecular pathways. Through manipulation of bioelectric signals, we will be able to activate full genetic cascades that result in the formation of multiple structures of the correct size and scale. Given that many ion transporter modulators are already approved for clinical use, this knowledge is likely to be beneficial for developing techniques in regenerative medicine.

Author Contributions

FD and ML designed the experiments and interpreted results. FD and JB performed and analyzed experimental data. CF created the model and wrote the modeling sections of the manuscript. JM performed the cloning, the *in situ* hybridizations, and the dsRNAi injections. JL and JB assisted with all membrane voltage imaging and drug treatments. AH repeated drug treatment experiments, including imaging, and increased number of samples. FD, ML, JB and CF wrote the manuscript with feedback from all authors.

Acknowledgments

We thank the members of the Levin lab, Alexis Pietak, and many researchers in the planarian regeneration community for useful discussions. We thank Anna Kane and Joshua Finkelstein for their helpful feedback and support in the submission of this manuscript. We are grateful to J. S. Marchant who provided animals for this study. We also thank Hans Gonzembach and the diligent undergraduates including Hannah Stowe, Quynh Anh Phan, Si Kun Wang, Sara E. Mitchell, Tien Hoang, John Fernandez, and Carolyn H. Nguyen who have helped us tend to our worm colony. We gratefully acknowledge support by an Allen Discovery Center award from the Paul G. Allen Frontiers Group (No. 12171), the G. Harold and Leila Y. Mathers Charitable Foundation (No. TFU141), the Templeton World Charity Foundation (No. TWCF0089/AB55), and the National Science Foundation (NSF) (IGERT DGE-1144591).

Figure Legends

Figure 1. Anterior/Posterior differences in bioelectric signaling exist before the earliest asymmetrically expressed gene *notum* appears.

(A-B) V_{mem} reporter assay using $DiBAC_4(3)$. Images are pseudocolored blue-green-red. Brighter pixels (red) are most positively charged on the inside of cells relative to outside, i.e. relatively depolarized. Pixels of lower intensity (blue) are relatively hyperpolarized or more negatively charged on the inside of cells relative to outside. Green arrows indicate anterior blastema and blue arrows indicate posterior blastema. (A) Untreated wild type (WT) *Dugesia japonica* (DJ) fragments cut from the same worm 2 hours before $DiBAC_4(3)$ imaging. Boxes indicate paired wound sites that were once in the same location in the animal. Anterior facing blastemas on posterior fragments are significantly depolarized compared with posterior facing blastemas on anterior fragments, which were located in the same position in the whole worm prior to amputation ($p<0.05$, N=14, paired t test). (B) WT fragments in $DiBAC_4(3)$ at (a) 1 hour, (b) 7 hours, (c) 14 hours and (d) 21 hours after amputation with anterior blastema oriented towards the top and posterior blastema oriented to the bottom. (C) Quantification of $DiBAC_4(3)$ fluorescence intensity at the anterior and posterior blastema of the same individual fragments during regeneration at 3 hours (N=19), 6 hours (N=23), 18 hours (N=17), 24 hours (N=11), and 48 hours after cutting (N=24). Blastemas from the same fragment are connected by a line. * $p<0.05$, ** $p<0.01$, *** $p<0.005$, paired t-test. (D) Timeline indicating *notum* expression in WT regenerating DJ at (a) 0 hour, (b) 3 hours and (c) 6 hours post-amputation, as determined by *in situ* hybridization. See Supplemental Figure 1 for notum expression at later timepoints. Amputation plane indicated in red on the sketch. Each panel representative of a timepoint includes the posterior wound site of the anterior portion of an amputated worm (top) and the anterior wound site of the posterior portion of an amputated worm (bottom). Purple arrows indicate punctate expression pattern. White arrows mark the edge of the blastema with no

signal. Yellow boxes in Figure 1A demarcate regions of interest. Scale bars represent 1 mm throughout.

Figure 2. Nigericin and Monensin treatment depolarizes worm fragments and leads to regeneration of double-headed planaria.

(A) Treatment timeline for ionophore (nigericin and monensin) solutions. PT fragments were amputated from WT *Dugesia japonica* and treated with 0.24μM nigericin + 15mM potassium gluconate, or with 0.08 μM monensin + 90 mM sodium gluconate for the first 3 hours post-amputation side by side with corresponding ethanol in water controls. Animals were moved from treatment solutions into water and washed 3 times. Worms regenerated for 2 weeks before they were scored. (B-C) V_{mem} reporter assay using $DiBAC_4(3)$. Brighter signal indicates relative depolarization, while lower intensity indicates relatively hyperpolarized cells. Green arrows indicate anterior blastema and blue arrows indicate posterior blastema. (B) Treatment with Nigericin solution. (a) $DiBAC_4(3)$ stained control *D. japonica* PT fragment 3 hours post-amputation. (b+c) Regenerative outcome of the control treatment, showing a single-headed worm, with a head at the anterior (b) and a tail at the posterior (c). (d) $DiBAC_4(3)$-stained *D. japonica* PT fragment 3 hours post-amputation treated with nigericin solution, showing strong depolarization, (e+f) which results in 13% double-headed regenerative outcomes for worms, with a head both at the anterior (e) and the posterior (f) in significantly higher numbers than controls where this phenotype was not observed ($p<0.01$, N=132, Fisher's exact test). (g) Quantification of the overall average $DiBAC_4(3)$ fluorescence intensity difference of pairs of control fragments (n=22 pairs) and pairs of one nigericin-treated fragment with a side-by-side control (n=18 pairs) all 3 hours post amputation. * $p<0.05$, unpaired t-test. (C) Treatment with Monensin solution. (a) $DiBAC_4(3)$ stained control *D. japonica* PT fragment 3 hours post-amputation. (b+c) Regenerative outcome of the control treatment, showing a single-headed worm, with a head at the anterior (b) and a tail at the posterior (c). d) $DiBAC_4(3)$-stained *D. japonica* PT fragment 3 hours post-amputation treated with monensin solution, showing strong depolarization,

(e+f) which results in 12% double-headed regenerative outcomes for worms, with a head both at the anterior (e) and the posterior (f) in significantly higher numbers than controls where this phenotype was not observed ($p<0.01$, N=89, Fisher's exact test). (g) Quantification of the overall average $DiBAC_4(3)$ fluorescence intensity difference of pairs of control fragments (n=22 pairs) and pairs of one monensin-treated fragment with a side-by-side control (n=18 pairs), all 3 hours post amputation. ** $p<0.01$, N=18 each, unpaired t test. Scale bars represent 1 mm.

Figure 3. A Model Integrating Planarian Bioelectrics to Regenerative Outcomes.

(A) Cells at the surfaces of wound blastema (inserts) are predicted to measure the difference between their own depolarization ($V_{mem}(B)$) and the average depolarization ($V_{mem}(Int)$) of neighboring cells just interior to the wound blastema. If this difference is larger than some threshold value, the Brain/Head pathway is activated; if the difference is smaller than this threshold or negative, the Tail pathway is activated. Branching between pathways is modeled by logistic-function kinetics. Local mutual inhibition by Notum and β-catenin is active in otherwise-untreated WT animals. (B) Treatment with nigericin solution (symbolized by orange lightning bolt arrow) immediately after amputation depolarizes both wound blastema, leading to Brain/Head pathway activation and head regeneration at both wounds. Excessive blastema depolarization turns local mutual inhibition by Notum and β-catenin off.

Figure 4. A brief, 3-hour depolarization changes early expression of notum.

(A) $DiBAC_4(3)$-staining of PT fragments in controls treated for 3 hours with ethanol control solutions, imaged at (a) 3 hours and (b) 6 hours, focusing on relative intensity distributions at the anterior (green arrow) compared to posterior (blue arrow) blastema. This is compared to fragments treated for 3 hours after amputation in 0.24 μM nigericin + 15mM potassium gluconate, imaged at (c) 3 hours and (d) 6 hours. (B) Quantification of the average $DiBAC_4(3)$ fluorescence intensity at the anterior blastema (green dots) and posterior blastema (purple) in

the nigericin treated fragments at 3 hours ($p>0.5$, N=19, paired t-test) and 6 hours ($p<0.05$, N=23, paired t-test) post-amputation. Values for blastemas from the same fragment are connected with a line. * $p<0.05$, paired t-test. (C) Timeline of *notum* expression in control treated fragments at (a) 3 hours and (b) 6 hours post-amputation, as determined by *in situ* hybridization, showing asymmetric expression of *notum* at the anterior blastema at 6 hours. Compared to absence of *notum* expression in fragments treated with the depolarizing nigericin solution at (c) 3 hours and (d) 6 hours post-amputation. Purple arrows indicate punctate expression pattern. White arrows mark the edge of the blastema with no signal. Scale bars represent 1 mm throughout.

Figure 5. *β-catenin* RNAi induces double-headed planaria without depolarization

(A) Scheme showing *β-catenin* dsRNAi injection, which results in regeneration of double-headed planaria from cut fragments. (B) (a) Example image of a *β-catenin* dsRNAi-induced double-headed planarian, showing abnormal shapes and defects in remodeling towards a normal body shape during the course of regeneration, (b) compared to double-headed planaria induced by nigericin treatment and (c) one induced by combination of *β-catenin* dsRNAi and nigericin treatment. (C) $DiBAC_4(3)$ staining 3 hours post-amputation of a (a) wild type fragment and (b) a fragment from a *β-catenin* dsRNAi injected animal amputated 1 week after injection, showing no relative difference in the V_{mem} ($p>0.05$, paired t-test). (c) $DiBAC_4(3)$ staining of a fragment treated with nigericin. (D) Quantification of the difference between $DiBAC_4(3)$ intensity of *β-catenin* dsRNAi-injected fragments and their respective controls versus nigericin treated fragments relative and their respective controls. ** $p<0.01$, paired t-test, n=11. (E) Principal Component analysis of planarian shape comparing *β-catenin* RNAi regenerate double-headed planaria (orange) versus nigericin solution-treated regenerate double-headed planaria (red) and double-headed planaria induced by nigericin treatment of previously *β-catenin* RNAi-injected worms (purple). Graphical output showing confidence ellipses for means, at a 0.95 probability, of shape data from the three treatment groups (n=18 *β-catenin* dsRNAi only, n=22

β-catenin dsRNAi + nigericin solution, n=14 nigericin solution alone). Differences in shape between groups subjected to *β-catenin* dsRNAi and the nigericin solution only treatment group were deemed significant with procrustes ANOVA ($p<0.0001$). Differences in shape between *β-catenin* dsRNAi and *β-catenin* dsRNAi + nigericin solution were not significant (procrustes ANOVA, $p>0.05$) (F) Example image of a double-headed worm with landmarks used for shape analysis marked. Scale bars represent 1 mm.

References

1. Cebrià, F. 2008. Organization of the nervous system in the model planarian Schmidtea mediterranea: An immunocytochemical study. Neuroscience Research 61(4):375-384.
2. Cebrià, F. 2007. Regenerating the central nervous system: how easy for planarians! Development genes and evolution 217(11-12):733-748.
3. Cebrià, F., T. Kudome, M. Nakazawa, K. Mineta, and K. Ikeo. 2002. The expression of neural-specific genes reveals the structural and molecular complexity of the planarian central nervous system. Mech. Dev. 116:199.
4. Cebrià, F., M. Nakazawa, K. Mineta, K. Ikeo, T. Gojobori, and K. Agata. 2002. Dissecting planarian central nervous system regeneration by the expression of neural-specific genes. Dev. Growth Differ. 44:135.
5. Morgan, T. 1898. Experimental studies of the regeneration of Planaria maculata. Development Genes and Evolution 7(2):364-397.
6. Salo, E., J. F. Abril, T. Adell, F. Cebria, K. Eckelt, E. Fernandez-Taboada, M. Handberg-Thorsager, M. Iglesias, M. D. Molina, and G. Rodriguez-Esteban. 2009. Planarian regeneration: achievements and future directions after 20 years of research. Int J Dev Biol 53(8-10):1317-1327.
7. Rink, J. 2013. Stem cell systems and regeneration in planaria. Development Genes and Evolution 223(1-2):67-84.
8. Aboobaker, A. A. 2011. Planarian stem cells: a simple paradigm for regeneration. Trends in Cell Biology 21(5):304-311.
9. Reddien, P. W., and A. S. n. Alvarado. 2004. Fundamentals of Planarian Regeneration. Annual Review of Cell and Developmental Biology 20(1):725-757.
10. Shibata, N., L. Rouhana, and K. Agata. 2010. Cellular and molecular dissection of pluripotent adult somatic stem cells in planarians. Development, growth & differentiation 52(1):27-41.
11. Durant, F., D. Lobo, J. Hammelman, and M. Levin. 2016. Physiological controls of large-scale patterning in planarian regeneration: a molecular and computational perspective on growth and form. Regeneration (Oxf) 3(2):78-102.
12. Levin, M., A. M. Pietak, and J. Bischof. 2018. Planarian regeneration as a model of anatomical homeostasis: Recent progress in biophysical and computational approaches. Semin Cell Dev Biol.
13. Owlarn, S., and K. Bartscherer. 2016. Go ahead, grow a head! A planarian's guide to anterior regeneration. Regeneration (Oxf) 3(3):139-155.
14. Umesono, Y., J. Tasaki, Y. Nishimura, M. Hrouda, E. Kawaguchi, S. Yazawa, O. Nishimura, K. Hosoda, T. Inoue, and K. Agata. 2013. The molecular logic for planarian regeneration along the anterior-posterior axis. Nature 500(7460):73-76.
15. Petersen, C. P., and P. W. Reddien. 2009. Wnt signaling and the polarity of the primary body axis. Cell 139(6):1056-1068.
16. Umesono, Y., J. Tasaki, Y. Nishimura, M. Hrouda, E. Kawaguchi, S. Yazawa, O. Nishimura, K. Hosoda, T. Inoue, and K. Agata. 2013. The

molecular logic for planarian regeneration along the anterior–posterior axis. Nature 500(7460):73.
17. Petersen, C. P., and P. W. Reddien. 2008. Smed-βcatenin-1 Is Required for Anteroposterior Blastema Polarity in Planarian Regeneration. Science 319(5861):327-330.
18. Gurley, K. A., J. C. Rink, and A. S. Alvarado. 2008. β-Catenin Defines Head Versus Tail Identity During Planarian Regeneration and Homeostasis. Science 319(5861):323-327.
19. Iglesias, M., J. L. Gomez-Skarmeta, E. Saló, and T. Adell. 2008. Silencing of Smed-βcatenin1 generates radial-like hypercephalized planarians. Development 135(7):1215-1221.
20. Petersen, C. P., and P. W. Reddien. 2009. A wound-induced Wnt expression program controls planarian regeneration polarity. Proceedings of the National Academy of Sciences 106(40):17061-17066.
21. Adell, T., E. Salò, M. Boutros, and K. Bartscherer. 2009. Smed-Evi/Wntless is required for β-catenin-dependent and-independent processes during planarian regeneration. Development 136(6):905-910.
22. Gurley, K. A., S. A. Elliott, O. Simakov, H. A. Schmidt, T. W. Holstein, and A. S. Alvarado. 2010. Expression of secreted Wnt pathway components reveals unexpected complexity of the planarian amputation response. Developmental biology 347(1):24-39.
23. Iglesias, M., M. Almuedo-Castillo, A. A. Aboobaker, and E. Saló. 2011. Early planarian brain regeneration is independent of blastema polarity mediated by the Wnt/β-catenin pathway. Developmental Biology 358(1):68-78.
24. Rink, J. C., K. A. Gurley, S. A. Elliott, and A. S. Alvarado. 2009. Planarian Hh signaling regulates regeneration polarity and links Hh pathway evolution to cilia. science 326(5958):1406-1410.
25. Yazawa, S., Y. Umesono, T. Hayashi, H. Tarui, and K. Agata. 2009. Planarian Hedgehog/Patched establishes anterior–posterior polarity by regulating Wnt signaling. Proceedings of the National Academy of Sciences 106(52):22329-22334.
26. Gerlitz, O., and K. Basler. 2002. Wingful, an extracellular feedback inhibitor of Wingless. Genes & development 16(9):1055-1059.
27. Wurtzel, O., Lauren E. Cote, A. Poirier, R. Satija, A. Regev, and Peter W. Reddien. 2015. A Generic and Cell-Type-Specific Wound Response Precedes Regeneration in Planarians. Developmental Cell 35(5):632-645.
28. Petersen, C. P., and P. W. Reddien. 2011. Polarized notum Activation at Wounds Inhibits Wnt Function to Promote Planarian Head Regeneration. Science 332(6031):852.
29. Levin, M. 2006. Is the early left-right axis like a plant, a kidney, or a neuron? The integration of physiological signals in embryonic asymmetry. Birth Defects Res C Embryo Today 78(3):191-223.
30. Adams, D. S., K. R. Robinson, T. Fukumoto, S. Yuan, R. C. Albertson, P. Yelick, L. Kuo, M. McSweeney, and M. Levin. 2006. Early, H+-V-ATPase-

dependent proton flux is necessary for consistent left-right patterning of non-mammalian vertebrates. Development 133:1657-1671.
31. Levin, M., T. Thorlin, K. R. Robinson, T. Nogi, and M. Mercola. 2002. Asymmetries in H+/K+-ATPase and cell membrane potentials comprise a very early step in left-right patterning. Cell 111(1):77-89.
32. Levin, M., Pezzulo, G., and Finkelstein, J. M. 2017. Endogenous Bioelectric Signaling Networks: Exploiting Voltage Gradients for Control of Growth and Form. Annual Review of Biomedical Engineering 19:353-387.
33. McLaughlin, K. A., and M. Levin. 2018. Bioelectric signaling in regeneration: Mechanisms of ionic controls of growth and form. Dev Biol 433(2):177-189.
34. Bates, E. 2015. Ion Channels in Development and Cancer. Annu Rev Cell Dev Biol 31:231-247.
35. Hyman, L. H. 1932. Studies on the correlation between metabolic gradients, electrical gradients, and galvanotaxis. II. Galvanotaxis of the brown Hydra and some non-fissioning planarians. Physiological Zoology 5(2):185-190.
36. Bonaventure, N. 1957. Galvanotropisme De Regenerats Monstrueux De Planaires-Monstres Bifides Et Heteromorphoses. Comptes Rendus Des Seances De La Societe De Biologie Et De Ses Filiales 151(3):598-602.
37. Lange, C. S., and V. E. Steele. 1978. The Mechanism of Anterior-Posterior Polarity Control in Planarians. Differentiation 11(1–3):1-12.
38. Marsh, G., and H. W. Beams. 1952. Electrical control of morphogenesis in regenerating dugesia tigrina. I. Relation of axial polarity to field strength. J Cell Comp Physiol 39(2):191-213.
39. Dimmitt, J., and G. Marsh. 1952. Electrical control of morphogenesis in regenerating Dugesia tigrina. II. Potential gradient vs. current density as control factors. J. Cell. Comp. Physiol. 40:11.
40. Durant, F., J. Morokuma, C. Fields, K. Williams, D. S. Adams, and M. Levin. 2017. Long-Term, Stochastic Editing of Regenerative Anatomy via Targeting Endogenous Bioelectric Gradients. Biophysical Journal 112(10):2231-2243.
41. Beane, W. S., J. Morokuma, D. S. Adams, and M. Levin. 2011. A Chemical genetics approach reveals H,K-ATPase-mediated membrane voltage is required for planarian head regeneration. Chemistry & Biology 18(1):77-89.
42. Oviedo, N. J., C. L. Nicolas, D. S. Adams, and M. Levin. 2008. Live Imaging of Planarian Membrane Potential Using DiBAC4(3). Cold Spring Harbor Protocols 2008(10):pdb.prot5055.
43. Barghouth, P. G., M. Thiruvalluvan, and N. J. Oviedo. 2015. Bioelectrical regulation of cell cycle and the planarian model system. Biochimica et Biophysica Acta (BBA)-Biomembranes 1848(10):2629-2637.
44. Emmons-Bell, M., F. Durant, J. Hammelman, N. Bessonov, V. Volpert, J. Morokuma, K. Pinet, D. S. Adams, A. Pietak, and D. Lobo. 2015. Gap Junctional Blockade Stochastically Induces Different Species-Specific Head Anatomies in Genetically Wild-Type Girardia dorotocephala

Flatworms. International journal of molecular sciences 16(11):27865-27896.
45. Beane, W. S., J. Morokuma, J. M. Lemire, and M. Levin. 2013. Bioelectric signaling regulates head and organ size during planarian regeneration. Development 140(2):313-322.
46. Levin, M. 2014. Endogenous bioelectrical networks store non-genetic patterning information during development and regeneration. The Journal of physiology 592(11):2295-2305.
47. Oviedo, N. J., J. Morokuma, P. Walentek, I. P. Kema, and M. B. Gu. 2010. Long-range neural and gap junction protein-mediated cues control polarity during planarian regeneration. Dev. Biol. 339:188.
48. Nogi, T., and M. Levin. 2005. Characterization of innexin gene expression and functional roles of gap-junctional communication in planarian regeneration. Developmental Biology 287(2):314-335.
49. Bardon, K. M., S. Selfridge, D. S. Adams, R. A. Minns, R. Pawle, T. C. Adams, and L. Takiff. 2018. Synthesis of Water-Soluble Far-Red-Emitting Amphiphilic BODIPY Dyes. ACS omega 3(10):13195-13199.
50. Pearson, B. J., G. T. Eisenhoffer, K. A. Gurley, J. C. Rink, D. E. Miller, and A. Sánchez Alvarado. 2009. Formaldehyde-based whole-mount in situ hybridization method for planarians. Developmental Dynamics 238(2):443-450.
51. Chan, J. D., D. Zhang, X. Liu, M. Z. Zarowiecki, M. Berriman, and J. S. Marchant. 2016. Dataset for a Dugesia japonica de novo transcriptome assembly, utilized for defining the voltage-gated like ion channel superfamily. Data in brief 9:1044-1047.
52. Rouhana, L., J. A. Weiss, D. J. Forsthoefel, H. Lee, R. S. King, T. Inoue, N. Shibata, K. Agata, and P. A. Newmark. 2013. RNA interference by feeding in vitro–synthesized double-stranded RNA to planarians: Methodology and dynamics. Developmental Dynamics 242(6):718-730.
53. Oviedo, N. J., C. L. Nicolas, D. S. Adams, and M. Levin. 2008. Gene knockdown in planarians using RNA interference. CSH protocols 2008:pdb-prot5054.
54. Adams, D. S., A. Masi, and M. Levin. 2007. H+ pump-dependent changes in membrane voltage are an early mechanism necessary and sufficient to induce Xenopus tail regeneration. Development 134(7):1323-1335.
55. Dexter, J. P., M. B. Tamme, C. H. Lind, and E.-M. S. Collins. 2014. On-chip immobilization of planarians for in vivo imaging. Scientific reports 4:6388.
56. Schindelin, J., I. Arganda-Carreras, E. Frise, V. Kaynig, M. Longair, T. Pietzsch, S. Preibisch, C. Rueden, S. Saalfeld, and B. Schmid. 2012. Fiji: an open-source platform for biological-image analysis. Nature methods 9(7):676.
57. Schneider, C. A., W. S. Rasband, and K. W. Eliceiri. 2012. NIH Image to ImageJ: 25 years of Image Analysis. Nature methods 9(7):671-675.
58. Klingenberg, C. P. 2011. MorphoJ: an integrated software package for geometric morphometrics. Molecular Ecology Resources 11(2):353-357.

59. Roberts-Galbraith, R. H., and P. A. Newmark. 2013. Follistatin antagonizes activin signaling and acts with notum to direct planarian head regeneration. Proceedings of the National Academy of Sciences of the United States of America 110(4):1363-1368.
60. Petersen, C. P., and P. W. Reddien. 2011. Polarized notum activation at wounds inhibits Wnt function to promote planarian head regeneration. Science 332(6031):852-855.
61. Harold, F. M., K. H. Altendorf, and H. Hirata. 1974. Probing membrane transport mechanisms with ionophores. Annals of the New York Academy of Sciences 235(1):149-160.
62. Mollenhauer, H. H., D. James Morré, and L. D. Rowe. 1990. Alteration of intracellular traffic by monensin; mechanism, specificity and relationship to toxicity. Biochimica et Biophysica Acta (BBA) - Reviews on Biomembranes 1031(2):225-246.
63. Chan, J. D., D. Zhang, X. Liu, M. Zarowiecki, M. Berriman, and J. S. Marchant. 2017. Utilizing the planarian voltage-gated ion channel transcriptome to resolve a role for a Ca2+ channel in neuromuscular function and regeneration. Biochimica et Biophysica Acta (BBA)-Molecular Cell Research 1864(6):1036-1045.
64. Chan, J. D., P. N. Agbedanu, M. Zamanian, S. M. Gruba, C. L. Haynes, T. A. Day, and J. S. Marchant. 2014. “Death and axes”: unexpected ca (2+) entry phenologs predict new anti-schistosomal agents. PLoS Pathog 10(2):e1003942.
65. Barish, M. E. 1983. A transient calcium-dependent chloride current in the immature Xenopus oocyte. The Journal of Physiology 342(1):309-325.
66. Carl, A., H. K. Lee, and K. M. Sanders. 1996. Regulation of ion channels in smooth muscles by calcium. American Journal of Physiology-Cell Physiology 271(1):C9-C34.
67. Ward, J. M., Pei Z-M, and J. I. Schroeder. 1995. Roles of ion channels in initiation of signal transduction in higher plants. Plant Cell 7(7):833-844.
68. Mathews, J., and M. Levin. 2017. Gap junctional signaling in pattern regulation: Physiological network connectivity instructs growth and form. Developmental neurobiology 77(5):643-673.
69. Palacios-Prado, N., S. Sonntag, V. A. Skeberdis, K. Willecke, and F. F. Bukauskas. 2009. Gating, permselectivity and pH-dependent modulation of channels formed by connexin57, a major connexin of horizontal cells in the mouse retina. J Physiol 587(13):3251-3269.
70. Palacios-Prado, N., and F. F. Bukauskas. 2009. Heterotypic gap junction channels as voltage-sensitive valves for intercellular signaling. Proc Natl Acad Sci U S A 106(35):14855-14860.
71. Oviedo, N. J., P. A. Newmark, and A. Sanchez Alvarado. 2003. Allometric scaling and proportion regulation in the freshwater planarian *Schmidtea mediterranea*. Dev Dyn 226(2):326-333.
72. Gonzalez-Estevez, C., and E. Salo. 2010. Autophagy and apoptosis in planarians. Apoptosis 15(3):279-292.

73. Potter, C. J., and T. Xu. 2001. Mechanisms of size control. Curr Opin Genet Dev 11(3):279-286.
74. Kucerova, R., P. Walczysko, B. Reid, J. Ou, L. J. Leiper, A. M. Rajnicek, C. D. McCaig, M. Zhao, and J. M. Collinson. 2011. The role of electrical signals in murine corneal wound re-epithelialization. Journal of cellular physiology 226(6):1544-1553.
75. Sebastian, A., S. A. Iqbal, J. Colthurst, S. W. Volk, and A. Bayat. 2015. Electrical stimulation enhances epidermal proliferation in human cutaneous wounds by modulating p53–SIVA1 interaction. Journal of Investigative Dermatology 135(4):1166-1174.
76. Zhang, W., and M. Bei. 2015. Kcnh2 and Kcnj8 interactively regulate skin wound healing and regeneration. Wound repair and regeneration 23(6):797-806.
77. Monteiro, J., R. Aires, J. D. Becker, A. Jacinto, A. C. Certal, and J. Rodríguez-León. 2014. V-ATPase proton pumping activity is required for adult zebrafish appendage regeneration. PloS one 9(3):e92594.
78. Adams, D. S., A.-S. Tseng, and M. Levin. 2013. Light-activation of the Archaerhodopsin H+-pump reverses age-dependent loss of vertebrate regeneration: sparking system-level controls in vivo. Biology open 2(3):306-313.
79. Pietak, A., and M. Levin. 2018. Bioelectrical control of positional information in development and regeneration: A review of conceptual and computational advances. Prog Biophys Mol Biol 137:52-68.
80. Mathews, J., and M. Levin. 2018. The body electric 2.0: recent advances in developmental bioelectricity for regenerative and synthetic bioengineering. Curr Opin Biotechnol 52:134-144.
81. Pai, V. P., A. Pietak, V. Willocq, B. Ye, N.-Q. Shi, and M. Levin. 2018. HCN2 Rescues brain defects by enforcing endogenous voltage pre-patterns. Nature communications 9(1):998.
82. Ardissone, A., V. Sansone, L. Colleoni, P. Bernasconi, and I. Moroni. 2017. Intrafamilial phenotypic variability in Andersen-Tawil syndrome: A diagnostic challenge in a potentially treatable condition. Neuromuscul. Disord. 27(3):294-297.
83. Levin, M., and C. J. Martyniuk. 2018. The bioelectric code: An ancient computational medium for dynamic control of growth and form. Biosystems 164:76-93.
84. Adams, D. S., S. G. Uzel, J. Akagi, D. Wlodkowic, V. Andreeva, P. C. Yelick, A. Devitt-Lee, J. F. Pare, and M. Levin. 2016. Bioelectric signalling via potassium channels: a mechanism for craniofacial dysmorphogenesis in KCNJ2-associated Andersen-Tawil Syndrome. J Physiol 594(12):3245-3270.
85. Masotti, A., P. Uva, L. Davis-Keppen, L. Basel-Vanagaite, L. Cohen, E. Pisaneschi, A. Celluzzi, P. Bencivenga, M. Fang, M. Tian, X. Xu, M. Cappa, and B. Dallapiccola. 2015. Keppen-Lubinsky Syndrome Is Caused by Mutations in the Inwardly Rectifying K(+) Channel Encoded by KCNJ6. Am J Hum Genet 96(2):295-300.

86. Kortüm, F., V. Caputo, C. K. Bauer, L. Stella, A. Ciolfi, M. Alawi, G. Bocchinfuso, E. Flex, S. Paolacci, and M. L. Dentici. 2015. Mutations in KCNH1 and ATP6V1B2 cause Zimmermann-Laband syndrome. Nature genetics 47(6):661.
87. Vandenberg, L. N., R. D. Morrie, and D. S. Adams. 2011. V-ATPase-dependent ectodermal voltage and ph regionalization are required for craniofacial morphogenesis. Developmental Dynamics 240(8):1889-1904.
88. Shi, R., and R. B. Borgens. 1995. Three-Dimensional Gradients of Voltage During Development of the Nervous System as Invisible Coordinates for the Establishment of Embryonic Pattern. Dev. Dyn. 202:101.
89. Meinhardt, H. 2009. Beta-catenin and axis formation in planarians. Bioessays 31(1):5-9.
90. Levin, M., G. Pezzulo, and J. M. Finkelstein. 2017. Endogenous bioelectric signaling networks: exploiting voltage gradients for control of growth and form. Annual review of biomedical engineering 19:353-387.
91. Perathoner, S., J. M. Daane, U. Henrion, G. Seebohm, C. W. Higdon, S. L. Johnson, C. Nusslein-Volhard, and M. P. Harris. 2014. Bioelectric signaling regulates size in zebrafish fins. PLoS genetics 10(1):e1004080.
92. Budunova, I. V., and L. A. Mittelman. 1992. The effect of K+/H+ antiporter nigericin on gap junction permeability. Cell biology and toxicology 8(1):63-73.
93. Daniele, R. P., S. K. Holian, and P. C. Nowell. 1978. A potassium ionophore (Nigericin) inhibits stimulation of human lymphocytes by mitogens. Journal of Experimental Medicine 147(2):571-581.
94. Pal, R., R. C. Gallo, and M. G. Sarngadharan. 1988. Processing of the structural proteins of human immunodeficiency virus type 1 in the presence of monensin and cerulenin. Proceedings of the National Academy of Sciences 85(23):9283-9286.
95. Brock, T. A., and J. B. Smith. 1982. Reversible stimulation of the Na+/K+ pump by monensin in cultures of vascular smooth muscle. Life sciences 31(10):1043-1050.
96. Zhang, W., and B. C. Kone. 2002. NF-κB inhibits transcription of the H+-K+-ATPase α2-subunit gene: role of histone deacetylases. American Journal of Physiology-Renal Physiology 283(5):F904-F911.
97. Yang, S. J., H. L. Liang, G. Ning, and M. T. T. Wong-Riley. 2004. Ultrastructural study of depolarization-induced translocation of NRF-2 transcription factor in cultured rat visual cortical neurons. European Journal of Neuroscience 19(5):1153-1162.
98. Levin, M. 2007. Large-scale biophysics: ion flows and regeneration. Trends Cell Biol. 17:262.
99. Law, R., and M. Levin. 2015. Bioelectric memory: modeling resting potential bistability in amphibian embryos and mammalian cells. Theor Biol Med Model 12(1):22.
100. Cervera, J., A. Pietak, M. Levin, and S. Mafe. 2018. Bioelectrical coupling in multicellular domains regulated by gap junctions: A conceptual approach. Bioelectrochemistry 123:45-61.

101. Gallaher, J., M. Bier, and J. S. van Heukelom. 2010. First order phase transition and hysteresis in a cell's maintenance of the membrane potential-An essential role for the inward potassium rectifiers. Biosystems 101(3):149-155.
102. Cervera, J., A. Alcaraz, and S. Mafe. 2014. Membrane potential bistability in nonexcitable cells as described by inward and outward voltage-gated ion channels. J Phys Chem B 118(43):12444-12450.
103. van Mil, H., J. Siegenbeek van Heukelom, and M. Bier. 2003. A bistable membrane potential at low extracellular potassium concentration. Biophys. Chem. 106(1):15-21.
104. Williams, S. R., S. R. Christensen, G. J. Stuart, and M. Hausser. 2002. Membrane potential bistability is controlled by the hyperpolarization-activated current I(H) in rat cerebellar Purkinje neurons in vitro. The Journal of physiology 539(Pt 2):469-483.
105. Zhang, W., and D. J. Linden. 2003. The other side of the engram: experience-driven changes in neuronal intrinsic excitability. Nature Reviews Neuroscience 4(11):885-900.
106. Herrera-Rincon, C., V. P. Pai, K. M. Moran, J. M. Lemire, and M. Levin. 2017. The brain is required for normal muscle and nerve patterning during early Xenopus development. Nat Commun 8(1):587.
107. Oizumi, M., S. Amari, T. Yanagawa, N. Fujii, and N. Tsuchiya. 2016. Measuring Integrated Information from the Decoding Perspective. PLoS computational biology 12(1):e1004654.
108. Tsien, J. Z., M. Li, R. Osan, G. Chen, L. Lin, P. L. Wang, S. Frey, J. Frey, D. Zhu, T. Liu, F. Zhao, and H. Kuang. 2013. On initial Brain Activity Mapping of episodic and semantic memory code in the hippocampus. Neurobiol. Learn. Mem. 105:200-210.

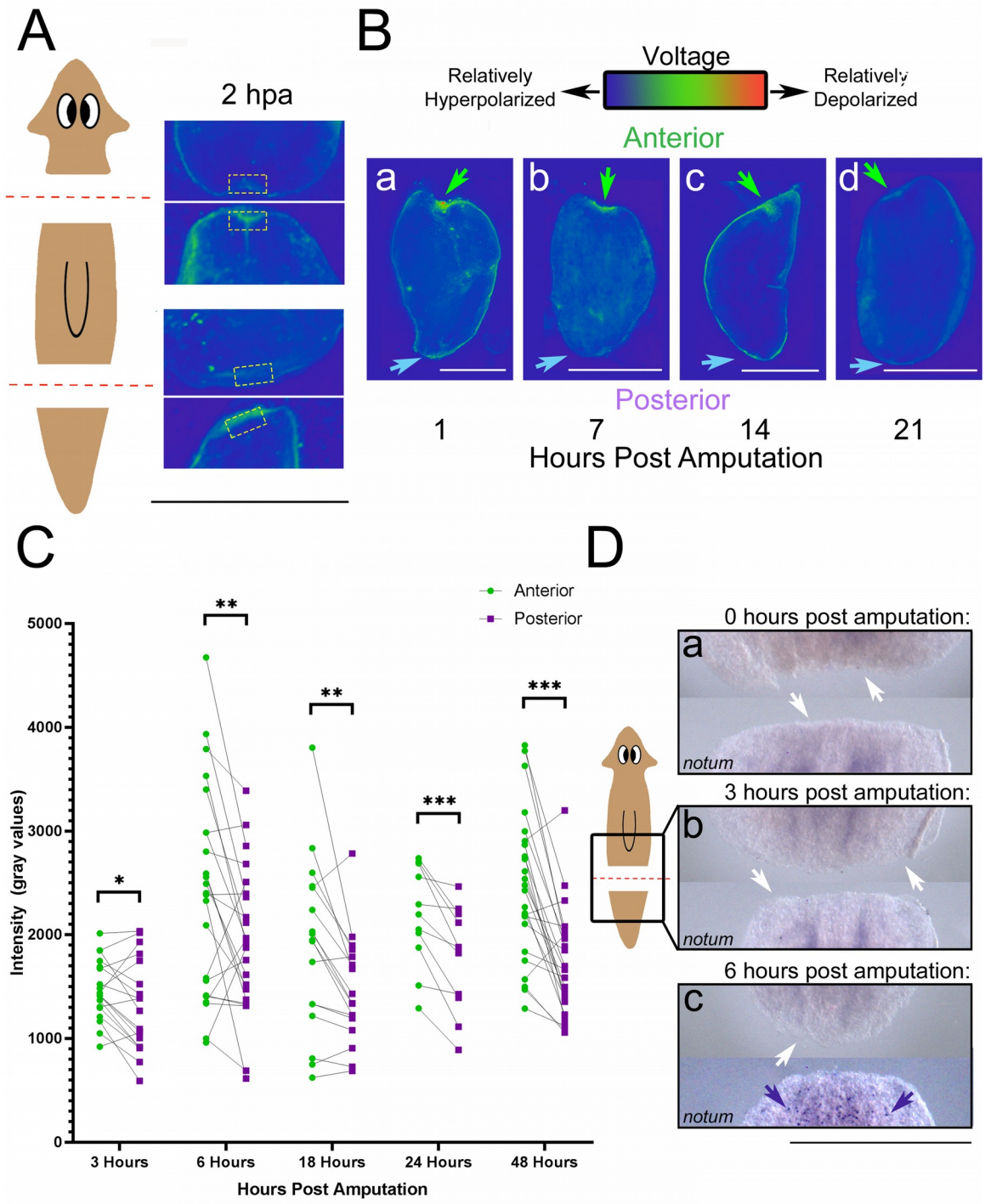
A
2 hpa
B
Voltage
Relatively Hyperpolarized
Relatively Depolarized
Anterior
a
b
c
d
Posterior
1
7
14
21
Hours Post Amputation
C
Anterior
Posterior
Intensity (gray values)
5000
4000
3000
2000
1000
0
*
**
**
***
***
3 Hours
6 Hours
18 Hours
24 Hours
48 Hours
Hours Post Amputation
D
0 hours post amputation:
a
notum
3 hours post amputation:
b
notum
6 hours post amputation:
c
notum

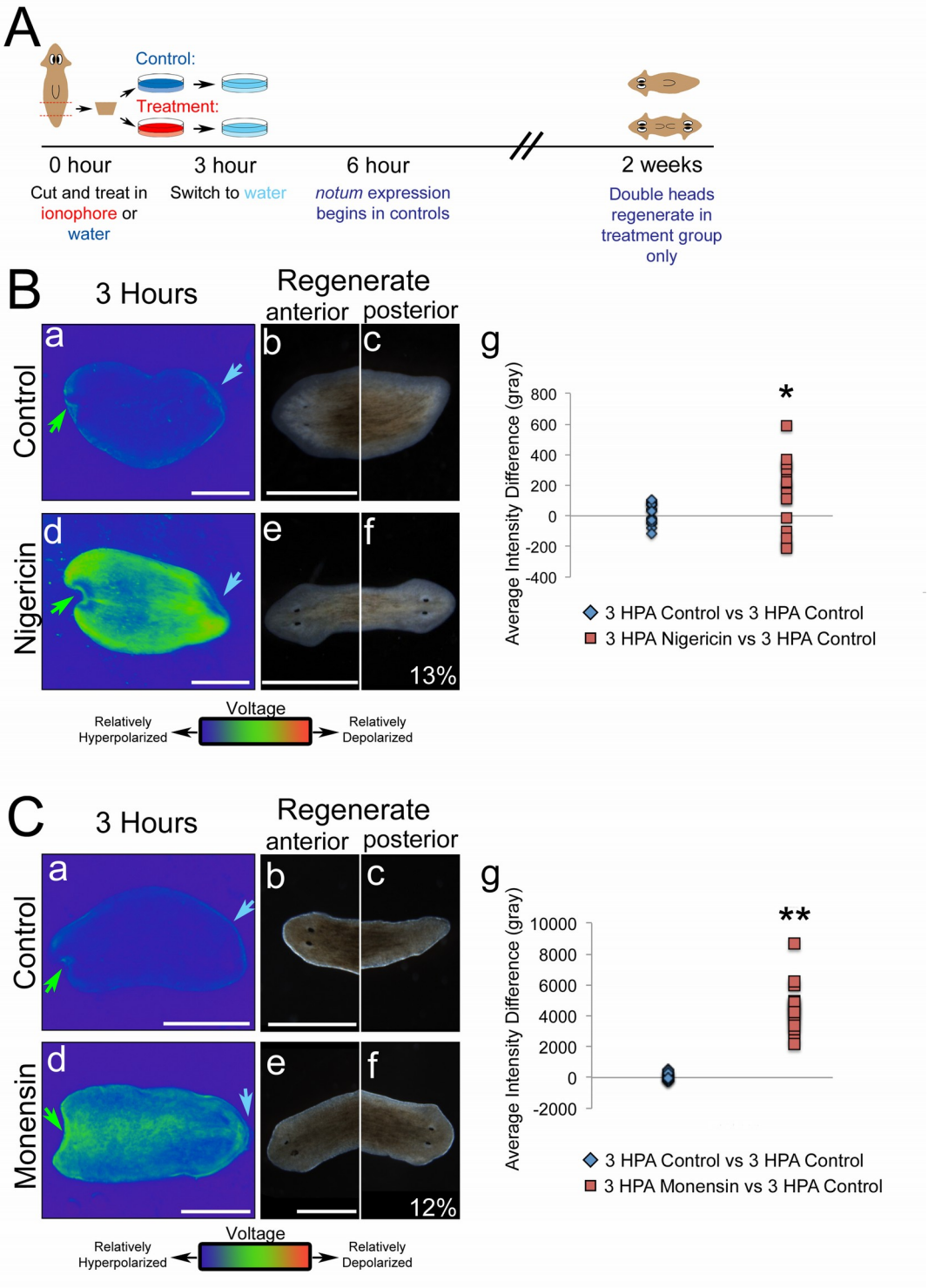
A
Control:
Treatment:
0 hour
Cut and treat in ionophore or water
3 hour
Switch to water
6 hour
notum expression begins in controls
2 weeks
Double heads regenerate in treatment group only
B
3 Hours
Regenerate
anterior
posterior
Control
Nigericin
a
b
c
d
e
f
13%
Voltage
Relatively Hyperpolarized
Relatively Depolarized
g
Average Intensity Difference (gray)
800
600
400
200
0
-200
-400
*
3 HPA Control vs 3 HPA Control
3 HPA Nigericin vs 3 HPA Control
C
3 Hours
Regenerate
anterior
posterior
Control
Monensin
a
b
c
d
e
f
12%
Voltage
Relatively Hyperpolarized
Relatively Depolarized
g
Average Intensity Difference (gray)
10000
8000
6000
4000
2000
0
-2000
**
3 HPA Control vs 3 HPA Control
3 HPA Monensin vs 3 HPA Control

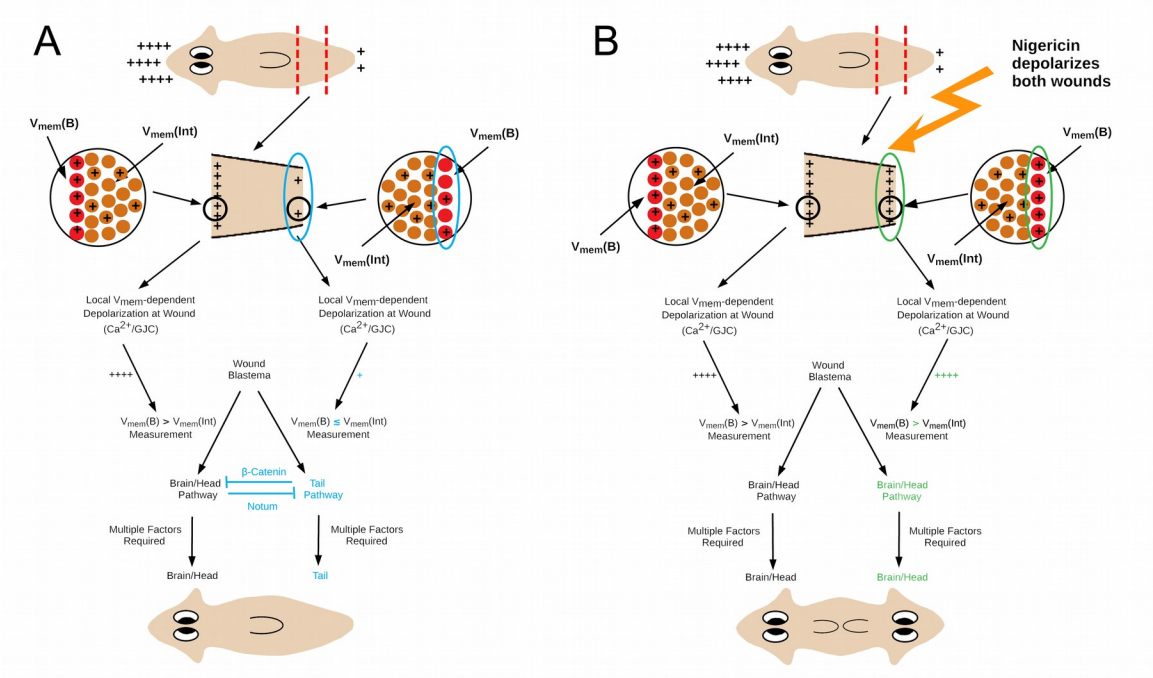
A
B
Nigericin depolarizes both wounds
Local Vmem-dependent Depolarization at Wound (Ca2+/GJC)
Wound Blastema
Vmem(B) > Vmem(Int) Measurement
Vmem(B) ≤ Vmem(Int) Measurement
Vmem(B) ≥ Vmem(Int) Measurement
β-Catenin
Brain/Head Pathway
Tail Pathway
Notum
Multiple Factors Required
Brain/Head
Tail

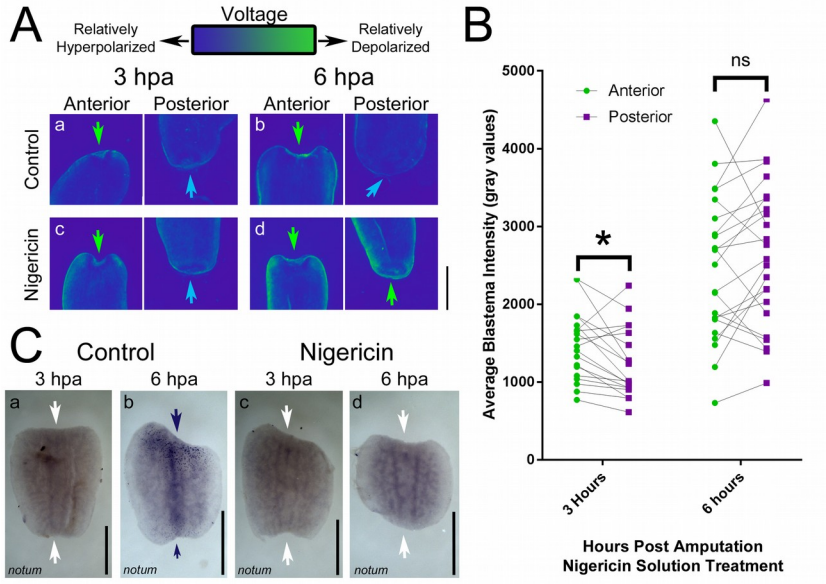
A
Voltage
Relatively Hyperpolarized
Relatively Depolarized
3 hpa
6 hpa
Anterior
Posterior
Control
Nigericin
B
Anterior
Posterior
ns
*
Average Blastema Intensity (gray values)
3 Hours
6 hours
Hours Post Amputation
Nigericin Solution Treatment
C
Control
Nigericin
notum

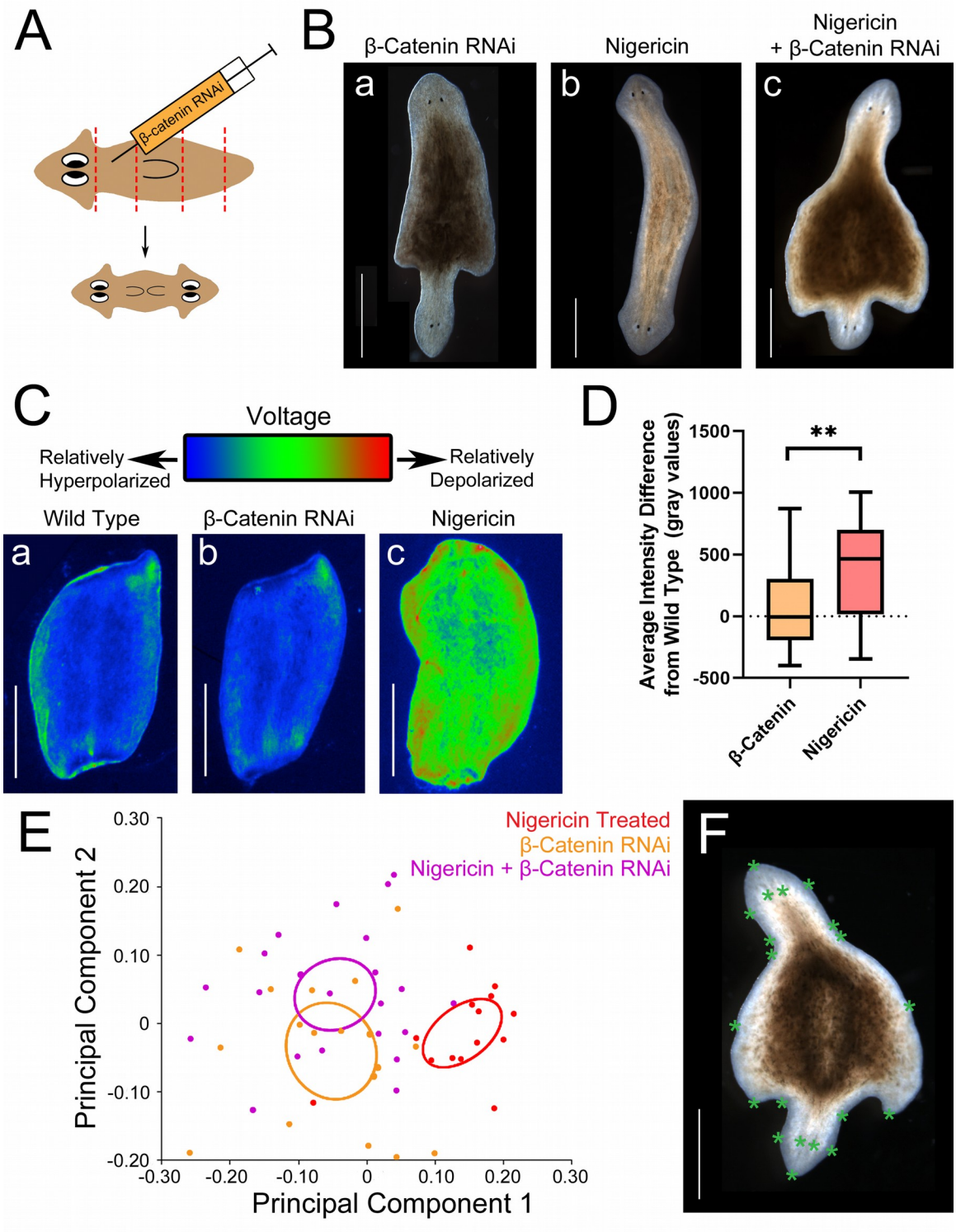
A
β-Catenin RNAi
B
β-Catenin RNAi
Nigericin
Nigericin
+ β-Catenin RNAi
a
b
c
C
Voltage
Relatively
Hyperpolarized
Relatively
Depolarized
Wild Type
β-Catenin RNAi
Nigericin
a
b
c
D
Average Intensity Difference
from Wild Type (gray values)
1500
1000
500
0
-500
**
β-Catenin
Nigericin
E
Nigericin Treated
β-Catenin RNAi
Nigericin + β-Catenin RNAi
Principal Component 2
0.30
0.20
0.10
0
-0.10
-0.20
-0.30
-0.20
-0.10
0
0.10
0.20
0.30
Principal Component 1
F